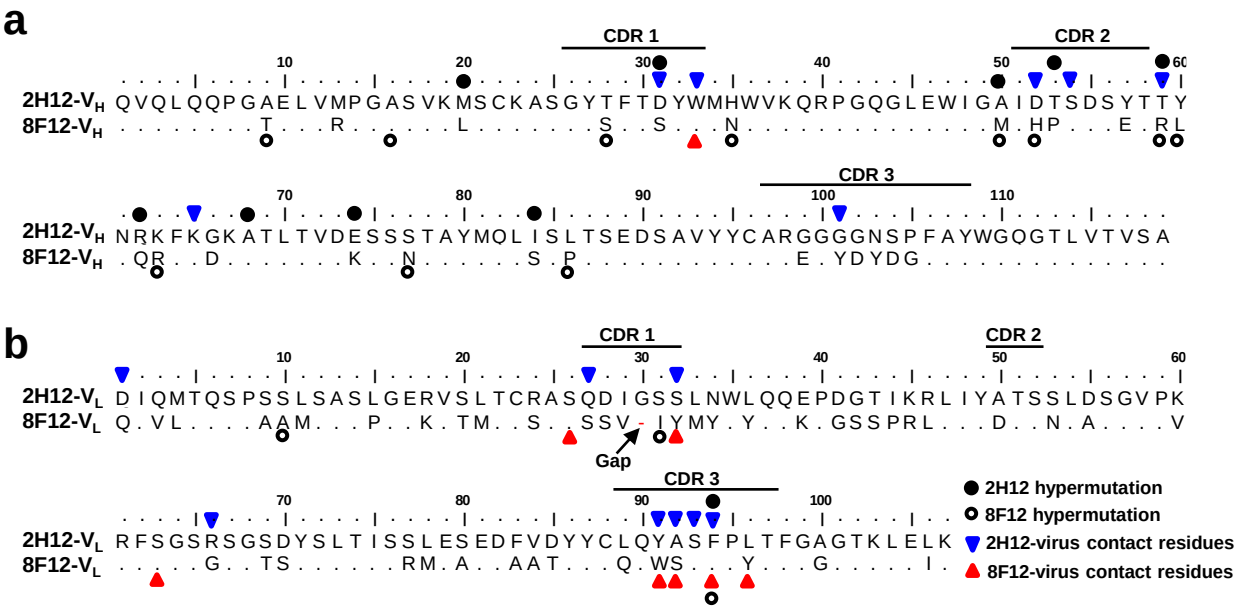

c

MAb	V-gene	D-gene	J-gene	Somatic hypermutation	Identity (%)
2H12-V_H	IGHV1-69*01	IGHD2-1*01	IGHJ3*01	9	92.4
2H12-V_L	IGKV9-120*01	—	IGKJ5*01	1	99.1
8F12-V_H	IGHV1-61*01	IGHD2-4*01	IGHJ3*01	11	90.8
8F12-V_L	IGKV4-55*01	—	IGKJ2*01	3	97.2

Supplementary Figure 1. Analysis of the MAb sequences. Variable domain-encoding sequences of both heavy and light chains of anti-EV-D68 MAbs were determined by 5‘ RACE assay. **(a, b)** Deduced amino acid sequences of heavy-chain variable regions (V_H) **(a)** and light-chain variable regions (V_L) **(b)** of the 2H12 and 8F12 MAbs. Dots represent residues identical to those of variable regions of the MAb 2H12, and red dashes are gaps. Locations of complementarity determining regions (CDR) were identified using the IgBLAST tool and indicated. Solid and hollow black spheres indicate positions of somatic hypermutation of antibodies 2H12 and 8F12, respectively. The 2H12-EV-D68 and 8F12-EV-D68 contact residues are indicated by blue inverted triangles and red triangles, respectively. **(c)** The closest mouse IgG germline genes were determined using the IgBLAST tool. The number of amino acid changes during antibody somatic hypermutation and the percentage of amino acid identity between our antibody sequences and germline sequences are also shown in this table.

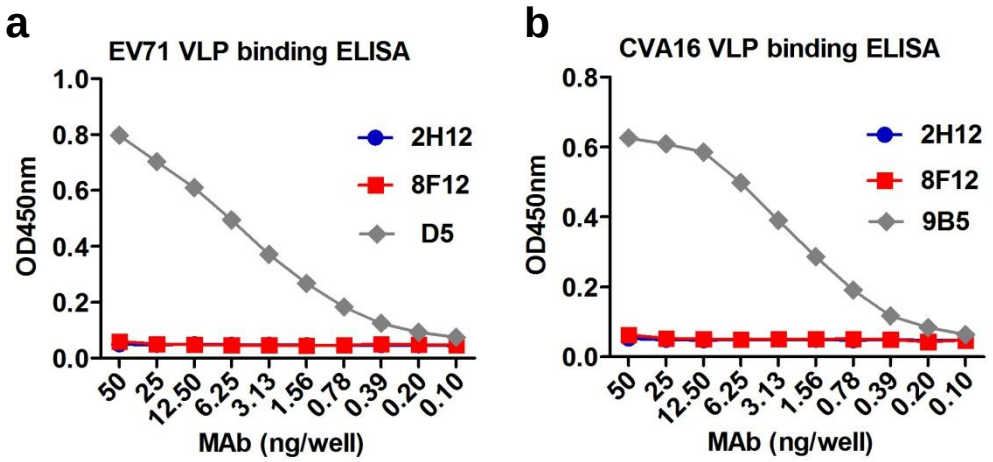

Supplementary Figure 2. Reactivities of anti-EV-D68 MAbs (2H12 and 8F12) towards EV71 VLP (a), and CVA16 VLP (b) determined by ELISA. Anti-EV71 MAb D5 and anti-CVA16 MAb 9B5 were used as positive controls for detection of EV71 VLP and CVA16 VLP, respectively.

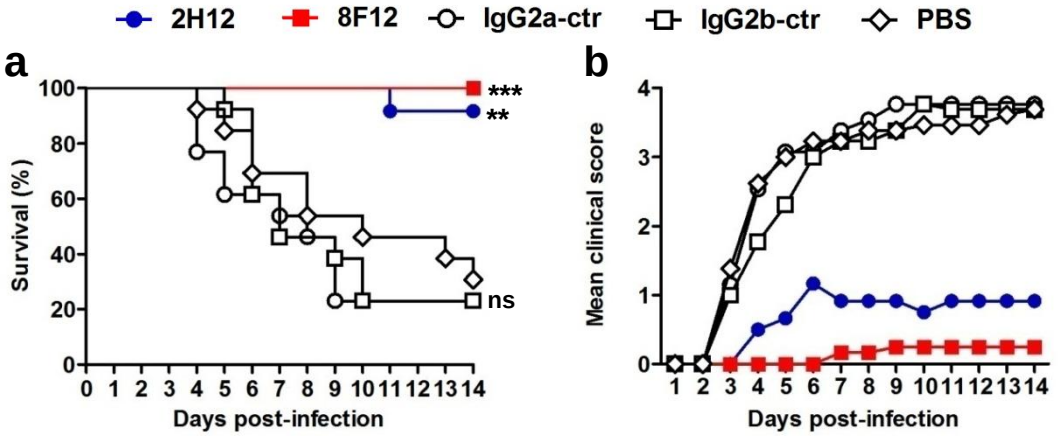

Supplementary Figure 3. Prophylactic efficacy of MAbs 2H12 and 8F12 against EV-D68 infection in neonatal mice. Groups of ICR mice (age < 24h; n = 12–14/group) were i.p. injected with PBS, 10 μg/g of 2H12, 8F12, IgG2a isotype control (ctr) MAb (1C11), or IgG2b isotype control MAb (1F4) and one day later challenged with strain 18947. The challenged mice were monitored daily for (**a**) survival and (**b**) clinical score. Clinical scores were graded as follows: 0, healthy; 1, lethargy and reduced mobility; 2, limb weakness; 3, limb paralysis; 4, death. Survival of mice in each antibody-treated groups was compared to the PBS control group. Statistical significance was indicated as follows: ns., no significant difference ($P \geq 0.05$); **, $P < 0.01$; ***, $P < 0.001$.

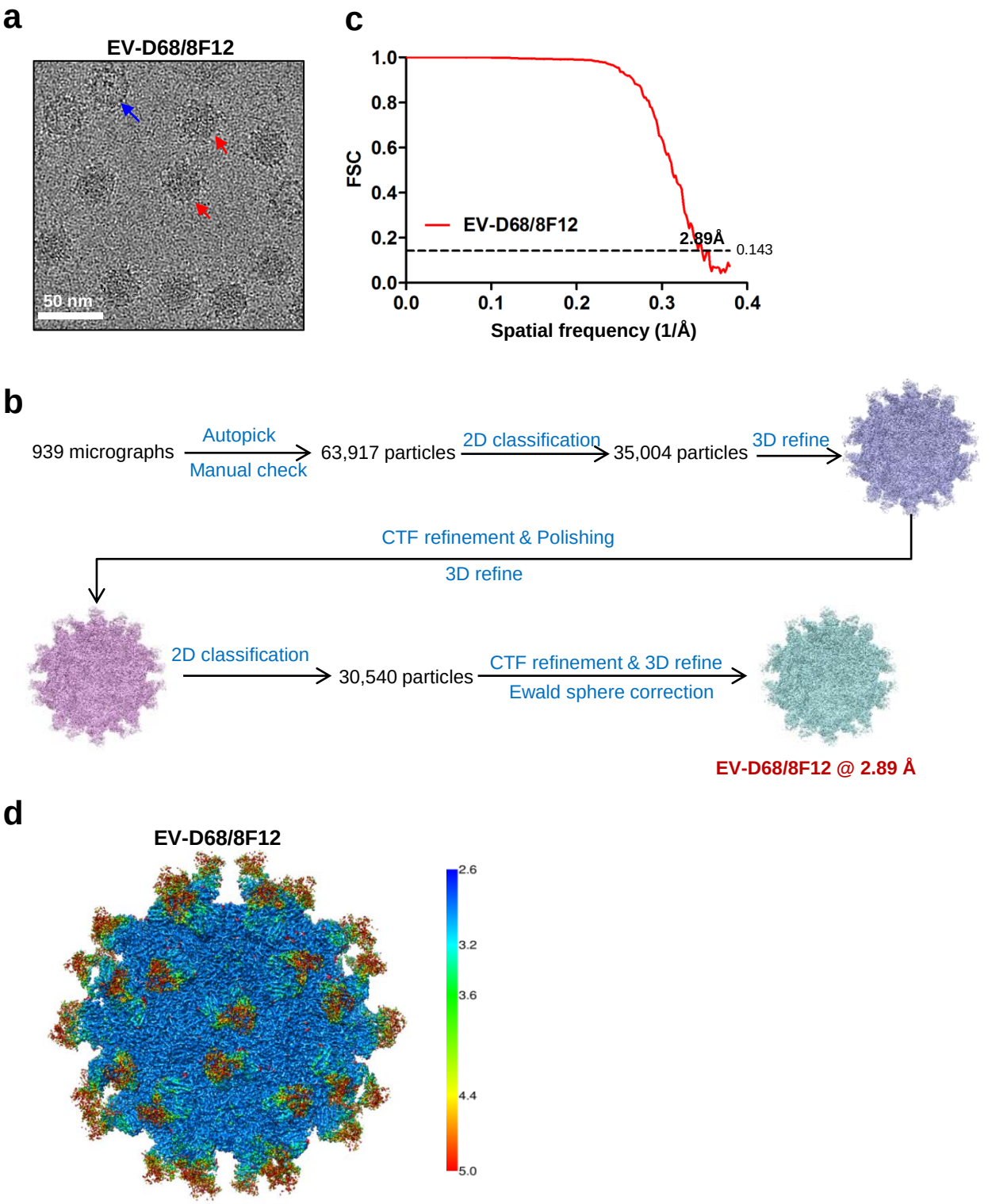

Supplementary Figure 4. Cryo-EM structural analysis of EV-D68/8F12 complex. (a) Cryo-EM images of the EV-D68/8F12 complex**.** Bar = 50 nm. Red and blue arrows indicate full and empty particles bound by the Fabs, respectively. **(b)** Flowchart of the 3D reconstruction process for the EV-D68/8F12 complex. **(c)** Resolution assessment of cryo-EM reconstructions of EV-D68/8F12 by Fourier shell correlation (FSC) at 0.143 criterion. **(d)** Local resolution evaluation of cryo-EM maps of EV-D68/8F12 by Relion 3.0. The resolution color bar (in Å) is also shown.

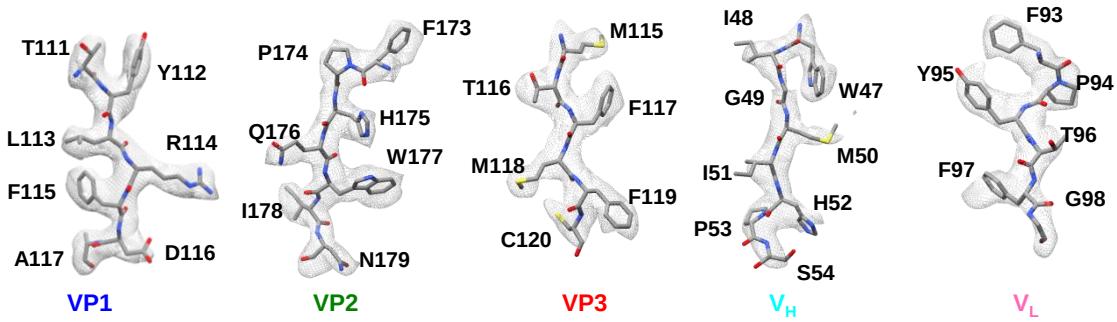

Supplementary Figure 5. Representative regions of density maps (mesh) of EV-D68/8F12 superimposed with their corresponding atomic models (sticks).

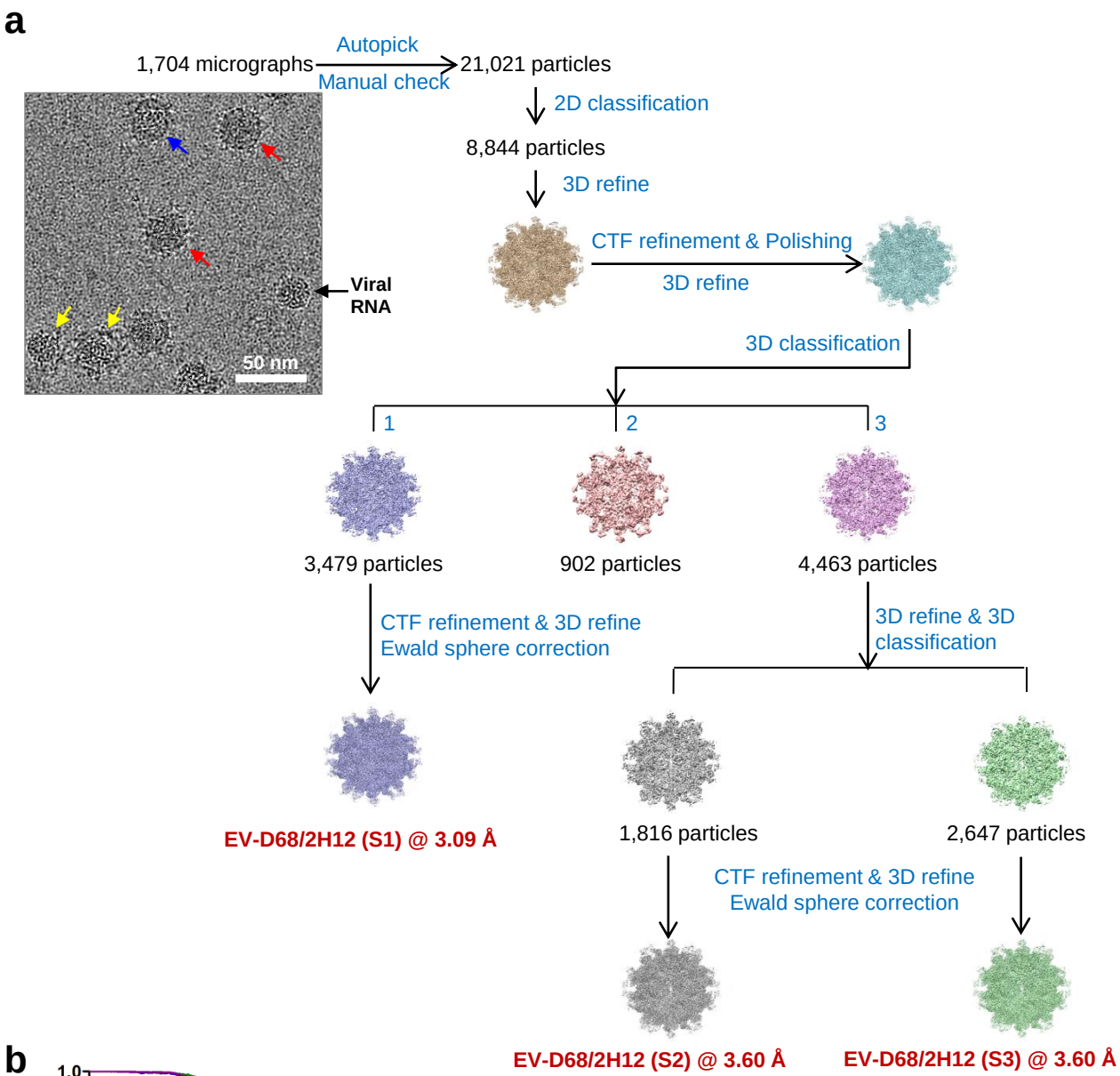
a
1,704 micrographs
Autopick
Manual check
21,021 particles
2D classification
8,844 particles
3D refine
CTF refinement & Polishing
3D refine
Viral RNA
50 nm
3D classification
1
2
3
3,479 particles
902 particles
4,463 particles
CTF refinement & 3D refine
Ewald sphere correction
3D refine & 3D classification
EV-D68/2H12 (S1) @ 3.09 Å
1,816 particles
2,647 particles
CTF refinement & 3D refine
Ewald sphere correction
EV-D68/2H12 (S2) @ 3.60 Å
EV-D68/2H12 (S3) @ 3.60 Å
b
FSC
1.0
0.8
0.6
0.4
0.2
0.0
0.0
0.1
0.2
0.3
0.4
3.60Å
3.09Å
0.143
EV-D68/2H12 (S1)
EV-D68/2H12 (S2)
EV-D68/2H12 (S3)
c
EV-D68/2H12 (S1)
EV-D68/2H12 (S2)
EV-D68/2H12 (S3)
2.6
3.2
3.6
4.4
5.0

Supplementary Figure 6. Cryo-EM structural analysis of EV-D68/2H12 complex. (a) Cryo-EM images of the EV-D68/2H12 complex and flowchart of the 3D reconstruction process for the EV-D68/2H12 complex**.** Bar = 50 nm. Red and blue arrows indicate full and empty particles bound by the Fabs, respectively. Yellow arrow indicates the broken particles induced by 2H12 binding. **(b)** Resolution assessment of cryo-EM reconstructions of EV-D68/2H12 by Fourier shell correlation (FSC) at 0.143 criterion. **(c)** Local resolution evaluation of cryo-EM maps of EV-D68/2H12 (states S1, S2, and S3) by Relion 3.0. The resolution color bar (in Å) is also shown.

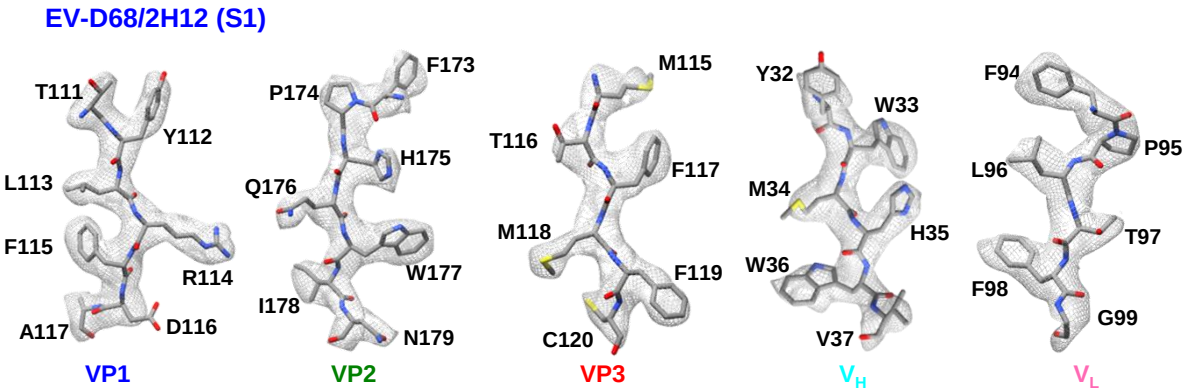

Supplementary Figure 7. Representative regions of density maps (mesh) of EV-D68/2H12 (S1) superimposed with their corresponding atomic models (sticks).

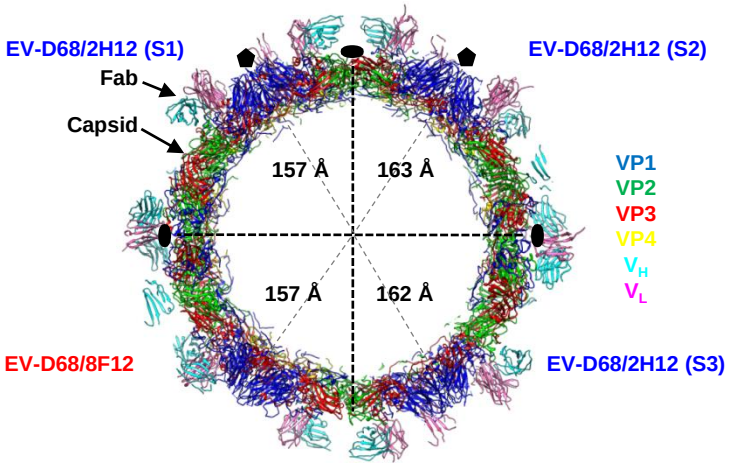

Supplementary Figure 8. Central slabs (ribbon) of EV-D68/8F12 and EV-D68/2H12 (states S1, S2, and S3) structures. Only one quarter of each structure is shown, to demonstrate the capsid expansion of EV-D68/2H12 S2 (top right) and S3 (bottom right) with respect to EV-D68/8F12 (bottom left) and EV-D68/2H12 S1 (top left). Radius of capsid shell of each structure is shown. Black oval and pentagon indicate locations of the two-fold and five-fold axes, respectively.